The effect of collision energy on the stereodynamics of the reaction $H(^2S) + NH(X^3\sum^-, v = 0, j = 0) \rightarrow N(^4S) + H_2$*

He Di(何 缔), Wang Mei-Shan(王美山)†, Yang Chuan-Lu(杨传路), and Jiang Zhi-Jun(姜志军)

School of Physics and Optoelectronic Engineering, Ludong University, Yantai 264025, *China*

(Received 11 September 2012; revised manuscript received 26 November 2012)

The quasi-classical trajectory (QCT) is calculated to study the stereodynamics properties of the title reaction $H(^2S) + NH(X^3\sum^-) \rightarrow N(^4S) + H_2$ on the ground state $^4A''$ potential energy surface (PES) constructed by Zhai and Han [2011 *J. Chem. Phys.* **135** 104314]. The calculated QCT reaction probabilities and cross sections are in good agreement with the previous theoretical results. The effects of the collision energy on the $\boldsymbol{k}$–$\boldsymbol{k}'$ distribution and the product polarization of H_2 are studied in detail. It is found that the scattering direction of the product is strongly dependent on the collision energy. With the increase in the collision energy, the scattering directions of the products change from backward scattering to forward scattering. The distribution of $P(\theta_r)$ is strongly dependent on the collision energy below the lower collision energy (about 11.53 kcal/mol). In addition, the $P(\phi_r)$ distribution dramatically changes as the collision energy increases. The calculated QCT results indicate that the collision energy plays an important role in determining the stereodynamics of the title reaction.

Keywords: stereodynamics, quasi-classical trajectory method, vector correlation, collision energy

PACS: 82.30.Cf, 82.20.Fd, 82.20.Hf, 82.20.Hf **DOI:** 10.1088/1674-1056/22/6/068201

1. Introduction

Nitrogen-containing compounds play an important role in atmospheric chemistry, the combustion of nitrogen-containing fuels, and explosion processes, which include a series of elementary reactions.[1–6] The ground-state hydrogen abstraction reaction $H(^2S) + NH(X^3\sum^-) \rightarrow N(^4S) + H_2$ is important among these elementary reactions. In recent decades, many experimental and theoretical studies have been devoted to this reaction. Experimentally, Morley[7] measured a rate constant value of $k = 1.02\times10^{13}$ cm^3·mol^{-1}·s^{-1} for the title reaction over the temperature range 1790 K–2200 K. This value was further recommended by Baulch *et al.*[8] in a temperature range of 1500 K–2500 K. In 1990, Koshi *et al.*[9] and Davidson and Hanson[10] investigated the $N(^4S) + H_2 \rightarrow H(^2S) + NH$ reaction using the direct detection of N atoms by the atomic resonance absorption technique in a shock tube apparatus at high temperature, and measured the rate coefficient in a temperature range of 1950 K–2850 K. Adam *et al.*[11] reported on the room-temperature rate constant $k = (1.92 \pm 0.5) \times 10^{13}$ cm^3·mol^{-1}·s^{-1} for the title reaction using quasi-static laser-flash photolysis and laser-induced fluorescence technology. Theoretically, Xu *et al.*[12] calculated the potential barrier and the heat of the reaction to be 1.68 kcal/mol and −28.95 kcal/mol at the MP-SAC4/6-311G** level of theory, respectively. Zhang and Truong[13] reported on the rate constants in a temperature range of 400 K–2500 K using microcanonical variational transition state theory (VTST), as well as the expression of the rate constant as $k(T) = 5.55 \times 10^8 T^{1.44} \exp(-0.78\ \text{(kcal/mol)/RT})$ cm^3·mol^{-1}·s^{-1}. In addition, the geometries of the transition state (TS) were presented by *ab initio* electronic structure calculations on the various levels of theory.

In the past few years, much effort has been made to construct the three-dimensional potential energy surface (PES) of the NH_2 system.[11,14–16] Pascual *et al.*[14] constructed a ground state PES $^4A''$ of the NH_2 system using a modified version of the GROW program in Refs. [17]– [20]. Moreover, they adopted the quasi-classical trajectory (QCT) method and VTST to theoretically determine the rate constant of the title reaction. Adam *et al.*[11] presented a semi-numerical PES by the multi-reference configuration interaction (MRCI) method and the augmented polarized quadruple zeta (aug-cc-pVQZ) basis set of Dunning.[21–25] At the same time, they calculated the cross section and rate constant of the title reaction using the QCT method. Poveda and Varandas[15] reported on a realistic global potential energy surface from double many-body expansion (DMBE) theory for the ground state of the NH_2 system based on the MRCI/aug-cc-pVQZ level. Han *et al.*[26] investigated the reaction probabilities, reaction cross section, and rotational alignment of the product employing the QCT and quantum mechanics calculations on the PES of Poveda and Varandas.[14] Recently, Zhai and Han[16] constructed a newer $^4A''$ PES (Zhai–Han PES) using the many-body expansion theory and the neural network (NN)[27] method from the high-quality *ab initio* data based on the MRCI/aug-cc-pV5Z level. Using Zhai–Han PES and the time-dependent quantum mechanics (TDQM) wave packet method, they obtained

*Project supported by the National Natural Science Foundation of China (Grant Nos. 11074103, 10974078, and 11174117) and the Discipline Construction Fund of Ludong University, China.

†Corresponding author. E-mail: mswang1971@163.com

© 2013 Chinese Physical Society and IOP Publishing Ltd

the reaction probabilities, integral reaction cross-sections, and rate constants for the title reaction. The calculated rate constants are in good agreement with the related experimental results.[7,11]

From the above-mentioned discussion, the construction of the PES of the NH_2 system and the investigation of its dynamical properties, such as the reaction probabilities, integral reaction cross sections, and rate constants, have made much progress. However, little has been reported about the stereodynamics properties of the title reaction. Besides, so far, there have been no answers as to how accurate the Zhai–Han PES can be and what the influence of the Zhai–Han PES on the dynamics properties of the title reaction is. In order to further verify the accuracy of the Zhai–Han PES and investigate the dynamics properties on account of the Zhai–Han PES, we employ the QCT method to study the stereodynamics properties of the title reaction. The remainder of the present paper is organized as follows. In Section 2 the basic theory is reviewed, and the results and discussion are shown in Section 3. Finally, some main conclusions are drawn in Section 4.

2. Basic theory

2.1. Quasiclassical trajectory calculations

In this work, the standard QCT method[28,29] is used to study the stereodynamics of the title reaction based on Zhai–Han PES.[16] The contours of the $^4A''$ PES for the linear arrangement are shown in Fig. 1. The reactants are prepared with the initial rotational and vibrational quantum numbers $j = 0$ and $v = 0$, respectively, while the collision energy ($E_{\rm col}$) ranges from 0.1 kcal/mol to 50.0 kcal/mol. Batches of 10^4 trajectories are sampled for the impact parameters from 0 to $b_{\rm max}$ and run for each collision energy. To ensure the conservation of the total energy and total angular momentum within an acceptable tolerance, the integration step size is fixed to be 0.1 fs. The trajectories are started and finished at a distance from the atom to the centre of mass (CM) of the diatom (30.0 Å, 1 Å = 0.1 nm) to ensure no interaction between them.

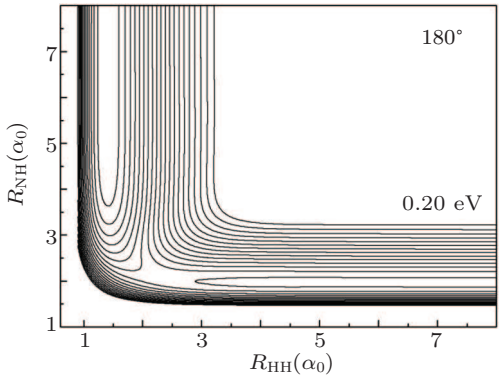


Fig. 1. The contours of the NH_2 PES in internal coordinates at $\theta_{\rm N-H-H} = 180°$. The figure is cited from Ref. [12].

2.2. Cross sections

In the framework of QCT, the total reactive cross section is defined as

$$\sigma_{\rm r} = \pi b_{\rm max}^2 \frac{N_{\rm r}}{N_{\rm T}}, \tag{1}$$

where $N_{\rm r}$ is the number of reactive trajectories and $N_{\rm T}$ is the total number of trajectories. The trajectories are run as a function of impact parameter b, which is sampled according to the formula $b^2 = \xi b_{\rm max}^2$, where ξ is a random number in the (0,1) interval. The sampling error is defined as $\sigma = \sqrt{(N_{\rm T} - N_{\rm r})/N_{\rm T}N_{\rm r}} \times 100\%$, and the uncertainty of the cross section may be estimated by

$$\Delta\sigma_{\rm r} = \sigma_{\rm r}\sigma. \tag{2}$$

2.3. Vector correlations

The CM frame is chosen to describe the directions of the various vectors, as shown in Fig. 2. The z axis is parallel to the relative velocity of the reagent $\boldsymbol{k}$, and the y axis is orthogonal to the x–z plane containing $\boldsymbol{k}$ and $\boldsymbol{k}'$ (the final relative velocity of the product). θ_t refers to the scattering angle between the vectors $\boldsymbol{k}'$ and $\boldsymbol{k}$, and θ_r and ϕ_r are the polar angle and azimuthal angle of the final rotational angular momentum $\boldsymbol{j}'$, respectively.

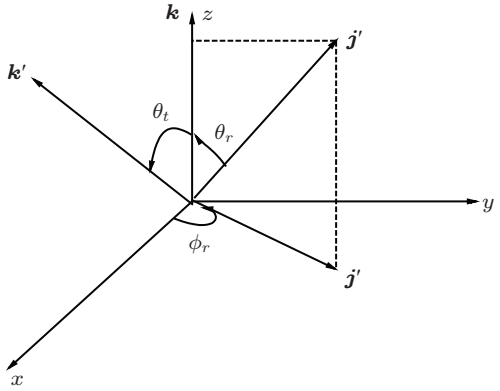


Fig. 2. The centre-of-mass coordinate system used to describe the $\boldsymbol{k}$–$\boldsymbol{k}'$–$\boldsymbol{j}'$ correlations.

The differential cross section (DCS), which describes the $\boldsymbol{k}$–$\boldsymbol{k}'$ distribution or the scattering direction of the product, is given by[29]

$$\frac{{\rm d}\sigma_R}{{\rm d}\omega} = \frac{\sigma_R}{2\pi}\left[\frac{1}{2} + \sum_n a_n {\rm P}_n(\cos\theta_t)\right], \tag{3}$$

where

$$a_n = \frac{2n+1}{2}\left\langle {\rm P}_n(\cos\theta_t)\right\rangle. \tag{4}$$

The distribution function $P(\theta_r)$, which describes the $\boldsymbol{k}$–$\boldsymbol{j}'$ correlation, can be expanded in a series of Legendre polynomials as follows:[30]

$$P(\theta_r) = \frac{1}{2}\sum_k (2k+1)a_0^{(k)}{\rm P}_k(\cos\theta_r), \tag{5}$$

where the coefficient $a_0^{(k)} = \int_0^{\pi} P(\theta_r) \mathrm{P}_k(\cos\theta_r) \sin\theta_r \mathrm{d}\theta_r = \langle \mathrm{P}_k(\cos\theta_r) \rangle$ is the polarization parameter. When k is odd, the polarization parameter is called the orientation parameter, and when k is even, it is called the alignment parameter. $k = 2$ indicates the rotational alignment of the product:

$$a_0^2 = \langle \mathrm{P}_2(\cos\theta_r) \rangle = \langle \mathrm{P}_2(j \cdot k) \rangle = \frac{1}{2} \langle 3\cos^2\theta_r - 1 \rangle. \quad (6)$$

The dihedral angle distribution function $P(\phi_r)$ describing $\boldsymbol{k}$–$\boldsymbol{k}'$–$\boldsymbol{j}'$ correlation can be expanded in a Fourier series as[31]

$$P(\phi_r) = \frac{1}{2\pi}(1 + \sum_{\text{even},n\geq 2} a_n \cos n\phi_r) + \sum_{\text{even},n\geq 1} b_n \sin n\phi_r, \quad (7)$$

where

$$a_n = 2\langle \cos n\phi_r \rangle \quad \text{and} \quad b_n = 2\langle \sin n\phi_r \rangle. \quad (8)$$

In the present work, $P(\phi_r)$ is expanded up to $n = 24$, which shows a good convergence.

The joint probability density function of angles θ_r and ϕ_r can be expressed by

$$\begin{aligned} & P(\theta_r, \phi_r) \\ &= \frac{1}{4\pi} \sum_{kq} [k] a_q^k C_{kq}(\theta_r, \phi_r)^* \\ &= \frac{1}{4\pi} \sum_k \sum_{q\geq 0} [a_{q\pm}^k \cos q\phi_r - a_{q\mp}^k \sin q\phi_r] C_{kq}(\theta_r, 0). \end{aligned} \quad (9)$$

The polarization parameter in our calculation is expressed as

$$a_{q\pm}^k = 2\langle C_{k|q|}(\theta_r, 0) \cos q\phi_r \rangle, \quad k \text{ is even}, \quad (10a)$$

$$a_{q\mp}^k = 2i\langle C_{k|q|}(\theta_r, 0) \sin q\phi_r \rangle, \quad k \text{ is odd}. \quad (10b)$$

$P(\theta_r, \phi_r)$ is expanded up to $k = 7$ in this calculation, which is sufficient for the good convergence.

3. Results and discussion

3.1. Reaction probabilities

Figure 3 presents the reaction probabilities for total angular momentum $\boldsymbol{J} = 0$ in a collision energy range of 0–20 kcal/mol. As the validity test for the present QCT calculations, the previous TDQM and QCT results[26] on DMBE PES are also shown in Fig. 3. It is easy to see that the QCT results overestimate the corresponding TDQM values near the threshold, mainly due to the problem of zero-point energy leakage.[32] At some collision energies, our QCT values are larger than the previous corresponding TDQM and QCT ones, which is mainly due to the fact that the PES employed by us is different from that by Han *et al.*[26] As a whole, our QCT results of the reaction probabilities are in good agreement with the previous results.[26] Therefore, one can conclude that the Zhai–Han PES is accurate and reliable for the study of the dynamic properties of the title reaction.

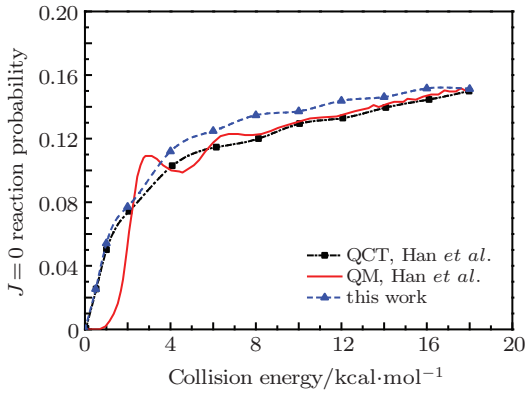


Fig. 3. (color online) A comparison between the QCT-computed reaction probability in this work and the other theoretical results for the $H(^2S) + NH(X^3\Sigma^-, v = 0, j = 0) \rightarrow N(^4S) + H_2$ reaction, where the solid line and the squares denote the QM results and QCT results of Han *et al.*,[26] respectively. The solid triangles refer to the QCT results in the present work.

3.2. Reactive cross section

Figure 4 shows the reactive cross sections for the $H(^2S) + NH(v = 0, j = 0) \rightarrow N(^4S) + H_2$ reaction, each as a function of the collision energy. Our QCT results are compared with the previous QCT and TDQM results.[11,16] As can be seen in Fig. 4, all the QM cross sections for this system are greater than the corresponding QCT results. As shown in Fig. 4, the QM-Coriolis coupling (QM-CC) results are smaller than the QM-centrifugal sudden (QM-CS) results at the higher collision energy. It is easy to see that the QCT results of this work are more consistent with the QM-CC results of Zhai and Han.[16] Furthermore, because of the barrier in the entrance channel, the cross sections evidently rise with increasing $\boldsymbol{E}_c$ before they reach their own plateau at around 20 kcal/mol.

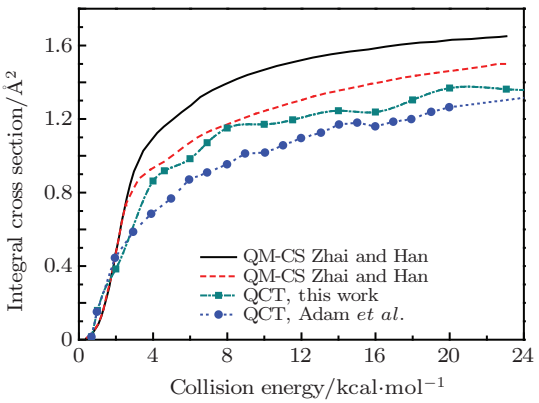


Fig. 4. (color online) Reactive cross sections, each as a function of the collision energy calculated for the $H(^2S) + NH(X^3\Sigma^-, v = 0, j = 0) \rightarrow N(^4S) + H_2$ reaction. The solid and dashed lines represent the QM-CS and QM-CC results of Zhai and Han,[16] respectively. The solid circles denote the QCT results of Adam *et al.*[11] The solid squares refer to the QCT results in the present work.

3.3. $\boldsymbol{k}$–$\boldsymbol{k}'$ vector correlations

Figure 5 shows the DCSs for the reaction $H(^2S) + NH(v = 0, j = 0) \rightarrow N(^4S) + H_2$ at the selected collision energies. Obviously, the H_2 molecules are scattered mainly in the backward hemisphere at a lower collision energy of 10 kcal/mol

and evolve from backward scattering to sideways scattering with increasing collision energy. At a higher collision energy of 50 kcal/mol, the $\boldsymbol{k}$–$\boldsymbol{k}'$ angular distributions are dominated by the sideways and forward scattering. This phenomenon correlates with an increase in $b_{\max}$, as well as an increasing fraction of reactive trajectories as the high initial impact parameters, when the collision energy rises.[33] Analysis of the dependences of the scattering angle on impact parameter and collision energy shows that the scattering in the forward hemisphere is produced only in reactive trajectories with high values of b. This is a consequence of the fact that the exploration of more repulsive regions of the PES, as collision energy rises, cannot counterbalance the increasing impulsive effect, which favors forward scattering.[16]

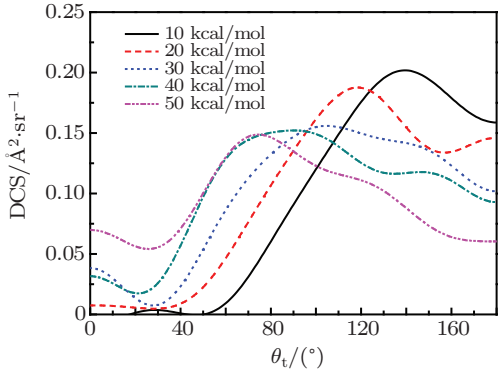


Fig. 5. (color online) Differential cross sections for the H(^{2}S) + NH ($X^3\Sigma^-$, $v = 0$, $j = 0$) → N(^{4}S) + H_2 reaction at five collision energies, plotted as a function of scattering angle θ_t.

3.4. $\boldsymbol{k}$–$\boldsymbol{j}'$ vector correlations

The $P(\theta_r)$ distributions of the product H_2 describe $\boldsymbol{k}$–$\boldsymbol{j}'$ correlations and reflect the rotational polarization of the H_2 product. Figure 6 shows the $P(\theta_r)$ distributions for the title reaction at six collision energies. It is clear that the $P(\theta_r)$ distributions peak at $\theta_r = 90°$ and are symmetric with respect to 90°, which shows that the rotational angular momentum vector of the product $\boldsymbol{j}'$ is strongly aligned along the direction at right angles with respect to the initial relative velocity direction. Further, one can find from Fig. 6 that the peak of the $P(\theta_r)$ distribution becomes stronger as the collision energy increases from 4.0 kcal/mol to 11.53 kcal/mol. Besides, it is easy to conclude from Fig. 6 that the effect of the collision energy on the $P(\theta_r)$ distribution is almost negligible in the range of the higher collision energy. The results elucidate that the rotational polarization of the H_2 product is steeply enhanced at collision energies below $\boldsymbol{E}_{\rm col} = 11.53$ kcal/mol. This phenomenon can be explained by the fact that the repulsive energy released by the title reaction in the exit channel causes the angular moment of the $\boldsymbol{j}'$ product to be preferentially perpendicular to the initial relative velocity direction with the increase in the collision energy. However, at a higher collision energy, the H(^{2}S) + NH ($X^3\Sigma^-$) → N(^{4}S) + H_2 reaction can be well simulated by the capture model, so most of the large repulsive energy that is released in the exit channel is converted into the intrinsic energy of the H_2 product. Therefore, one can conclude that the repulsive energy cannot make further contributions to the rotational polarization of the H_2 product when the collision energy is larger than 11.53 kcal/mol.

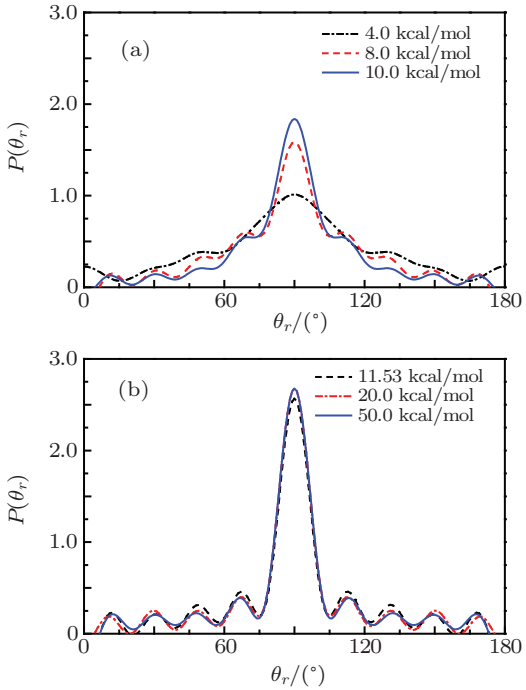


Fig. 6. (color online) Distributions of $P(\theta_r)$ for H(^{2}S) + NH ($X^3\Sigma^-$, $v = 0$, $j = 0$) → N(^{4}S) + H_2, reflecting $\boldsymbol{k}$–$\boldsymbol{j}'$ correlation at six collision energies $E_{\rm col} = 4.0$, 8.0, 10.0, 11.53, 20.0, 50.0 kcal/mol.

3.5. $\boldsymbol{k}$–$\boldsymbol{k}'$–$\boldsymbol{j}'$ vector correlations

The $P(\phi_r)$ distributions of the H_2 product shown in Fig. 7 describe $\boldsymbol{k}$–$\boldsymbol{k}'$–$\boldsymbol{j}'$ correlations at the six collision energies of 4.0, 8.0, 10.0 kcal/mol and 11.53, 20.0, 50.0 kcal/mol, respectively. The $P(\phi_r)$ distributions are asymmetric with respect to the $\boldsymbol{k}$–$\boldsymbol{k}'$ scattering plane. The peaks of $P(\phi_r)$ appearing at $\phi_r = 90°$ and $\phi_r = 270°$ not only show that the rotational angular momentum vectors of the products are mainly aligned along the y axis of the CM frame, but also that the reaction proceeds preferentially when the reactant velocity vector lies in a plane containing all three atoms. In all cases, the peak at $\phi_r = 270°$ is apparently stronger than that at $\phi_r = 90°$, which means that the rotational angular momentum vector of the product j' tends to be oriented along the negative direction of the y axis.

It is easy to find from Fig. 7 that the $P(\phi_r)$ distributions dramatically change as the collision energies increase, which means that the rotational polarization of H_2 is strongly dependent on the collision energy. More specifically, the degree of orientation becomes much stronger with the increase in collision energy in a collision energy range from 4.0 kcal/mol to 10.0 kcal/mol. However, the degree of orientation is much

weaker as the collision energy increases in a collision energy range from 11.53 kcal/mol to 50.0 kcal/mol.

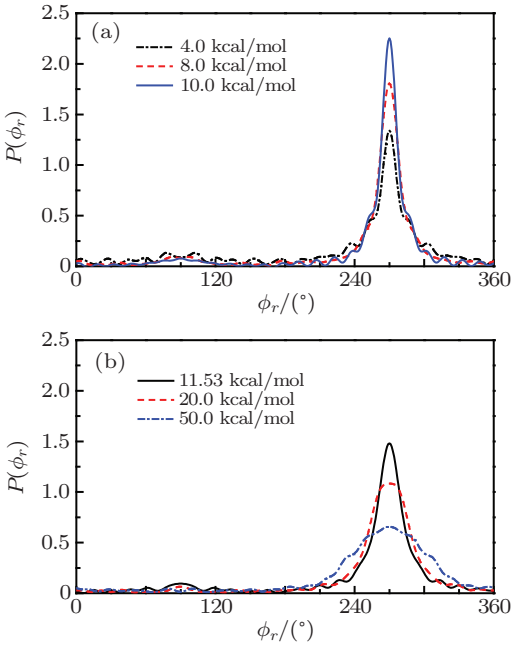


Fig. 7. (color online) Dihedral angle distributions of $P(\phi_r)$, describing the $\boldsymbol{k}$–$\boldsymbol{k}'$–$\boldsymbol{j}'$ correlation at six collision energies, $E_{\rm col}$ = 4.0, 8.0, 10.0, 11.53, 20.0, 50.0 kcal/mol.

Generally speaking, the effects of the collision energy on the orientation degree of a reaction monotonically change with increasing collision energy. Therefore, it is an interesting phenomenon that the influences of the relatively low collision energy and the relatively high collision energy on the product orientation of the title reaction are greatly different from each other. According to the impulsive model[29] of the reaction A + BC→ AB + C, the rotational angular momentum of the $\boldsymbol{j}'$ product can be expressed as

$$J' = L\sin^2\beta + J\cos^2\beta + J_1 m_{\rm B}/m_{\rm AB} \tag{11}$$

with

$$\cos^2\beta = m_{\rm A}m_{\rm C}/(m_{\rm A}+m_{\rm B})(m_{\rm B}+m_{\rm C}) \tag{12}$$

and

$$J_1 = (\mu_{\rm BC}\boldsymbol{E}_{\rm r})^{1/2}(\boldsymbol{r}_{\rm AB}\times\boldsymbol{r}_{\rm CB}), \tag{13}$$

where $\boldsymbol{L}$ and $\boldsymbol{J}$ are the orbital and rotational angular momentums of the reactant molecule AB, respectively; $\cos^2\beta$ is the mass factor; $\mu_{\rm BC}$ represents the reduced mass of the BC molecule; $\boldsymbol{E}_r$ is the repulsive energy; and $r_{\rm AB}$ and $r_{\rm CB}$ are unit vectors where B points to A and C, respectively. During the forming and breaking of the chemical bond for the title reactions, the term $L\sin^2\beta + J\cos^2\beta$ in Eq. (9) is symmetric with respect to the $\boldsymbol{k}'$–$\boldsymbol{k}$ scattering plane. However, $J_1 m_{\rm B}/m_{\rm AB}$ tends to a preferred direction because of the effect of the repulsive energy $\boldsymbol{E}_r$, which causes the orientation of the product molecule. The repulsive energy produces more H_2 molecules rotating clockwise in the scattering plane when the collision energy increases from 4.0 kcal/mol to 11.53 kcal/mol. However, the rotation preference of H_2 will change from the in-plane reaction mechanism to the out-of-plane mechanism when the collision energy is higher than 11.53 kcal/mol, which also means that the peaks of the $P(\phi_r)$ distributions at $\phi_r = 270^\circ$ become lower and broader. Figure 8 depicts the distributions of the $P(\theta_r, \phi_r)$ at collision energies of 10.0 kcal/mol and 50.0 kcal/mol, and the peaks at 90° and 270° are in good accordance with those of the distributions of $P(\theta_r)$ and $P(\phi_r)$.

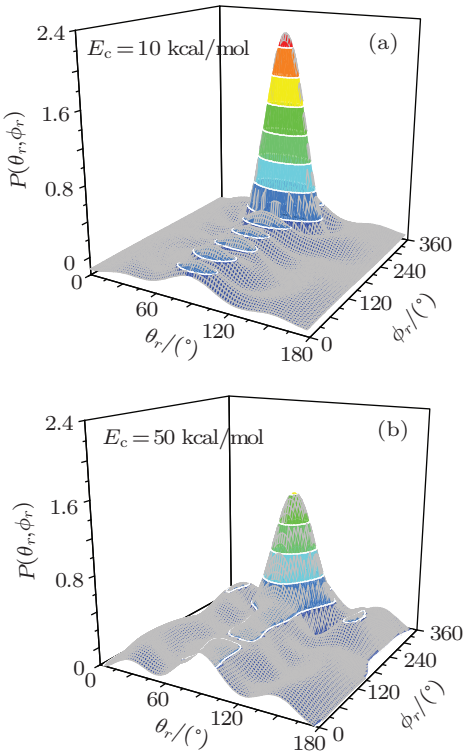


Fig. 8. (color online) Polar plots of $P(\theta_r, \phi_r)$ distribution averaged over all scattering angles for the H(^{2}S) + NH ($v = 0$, $j = 0$) →N(^{4}S) + H_2 reaction at two collision energies, $E_{\rm col}$ = 10.0 kcal/mol and 50.0 kcal/mol.

In order to gain a deep understanding of the reaction mechanism of the title reaction, we observe many reactive trajectories and analyze the evolutions of the three inter-nuclear distances with time. The variations in the internuclear distances of H_a–H_b, H_b–N, and H_a–N are presented each as a function of propagation time in Fig. 9. It is clear from Fig. 9 that the title reaction is dominated by the direct reaction mechanism and the collision time becomes shorter with the increment in collision energy. As a result of a small barrier in the entrance channel of the title reaction, a purely downhill takes its route to the products. Therefore, the long-lived collision complexes cannot form on the PES, and a direct dynamic dominates the whole collision process.

Based on the above analyses, a picture is presented to describe the relationship between the microscopic mechanism and the orientation of the $\boldsymbol{j}'$ vector in the CM frame. The top panels of Fig. 10 illustrate the trajectories at the low collision energy. When the reactants go through the saddle point, the H_2 molecule is scattered in the backward hemisphere and the $\boldsymbol{j}'$ rotates clockwise in the scattering plane due to the large repulsive energy that is released in the exit channel. As can be seen in the bottom panels of Fig. 10, during N–H_b bond breaking, the H_a atom, having a high kinetic energy, captures the H_b and scatters in the forward hemisphere.

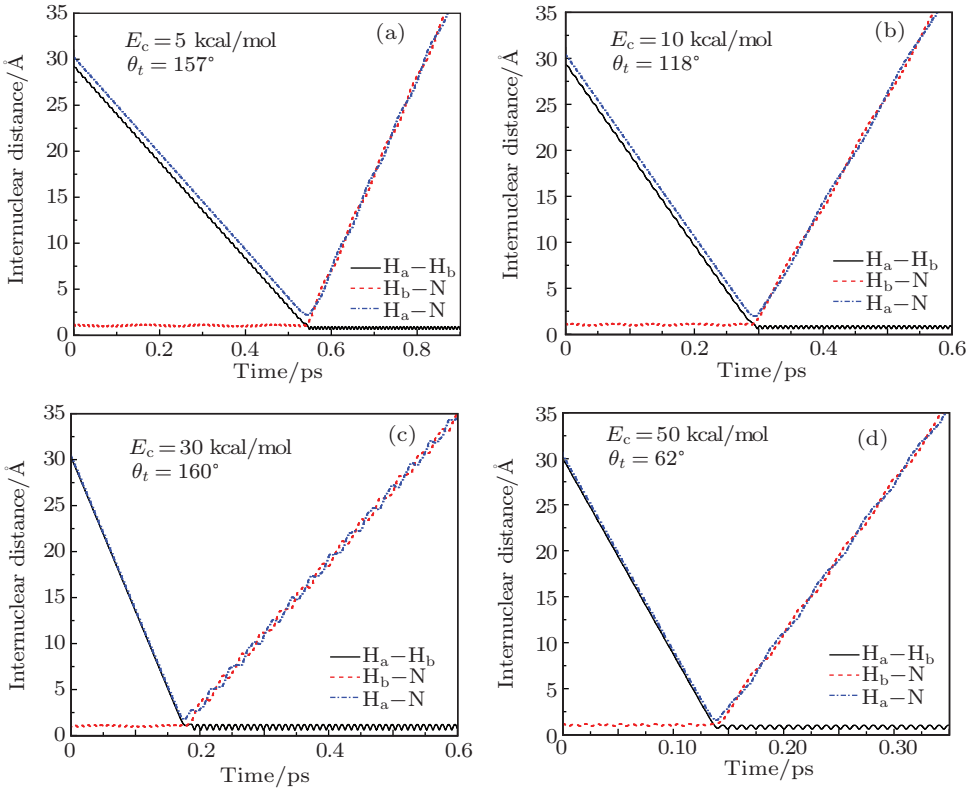


Fig. 9. (color online) Internuclear distances of H_a–H_b, H_b–N, and H_a–N, each as a function of propagation time, with scattering angles of $\theta_t = 157°$ at $E_c = 5$ kcal/mol (a), $\theta_t = 118°$ at $E_c = 10$ kcal/mol (b), $\theta_t = 160°$ at $E_c = 30$ kcal/mol (c), and $\theta_t = 62°$ at $E_c = 50$ kcal/mol (d).

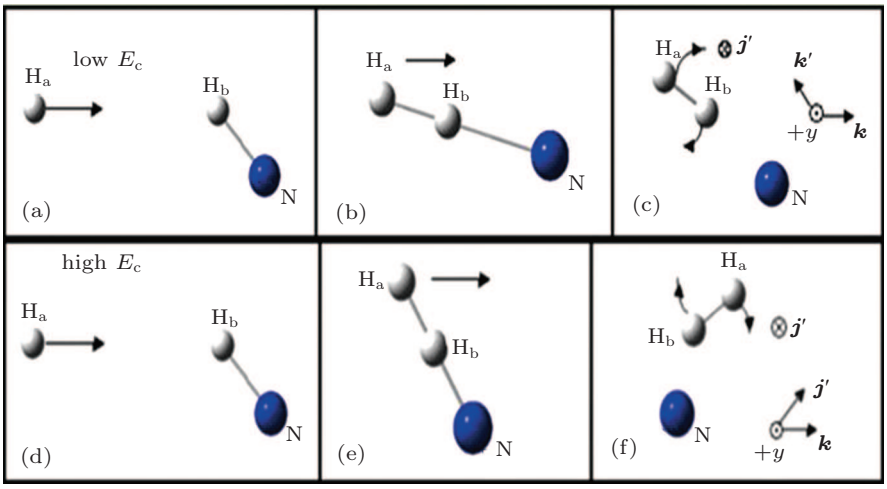


Fig. 10. (color online) Schematic illustration of two typical trajectories leading to $\boldsymbol{j}'$ orientation in the CM scattering frame. The top panels show the rebound reaction trajectories and the bottom panels show the stripping reaction trajectories.

4. Conclusions

In this paper, we use the QCT method to study the stereodynamics of the reaction $H(^2S) + NH(X^3\Sigma^-,\ v = 0,\ j = 0) \rightarrow N(^4S) + H_2$ taking place on the ground state the of NH_2 system. The influences of the collision energy on the total reaction cross section, the $\boldsymbol{k}'$–$\boldsymbol{k}$ vector correlation, and the

product polarization of the title reaction are investigated. It is found that the collision energy significantly enhances the reactive cross section. The product mainly tends to backward scattering at lower collision energies, but sideways and forward scattering emerge at higher collision energies. In a collision energy range of 4.0 kcal/mol–50.0 kcal/mol, the product rotational angular momentum vector j' is oriented along the negative direction of the y axis. The distributions of $P(\phi_r)$ for the title reaction indicate that the rebound reaction is dominated by an in-plane mechanism at the lower collision energy, while the stripping reaction is dominated by an out-of-plane mechanism at the higher collision energy. In all cases, the title reaction is dominated by the direct reaction mechanism and the collision time becomes shorter with the increase in collision energy.

Acknowledgment

All calculations were carried out in the Shuguang Super Computer Center (SSCC) of Ludong University. The authors also appreciate professor Han Ke-Li for providing the QCT code of the stereodynamics, as well as for some precious advice.

References

[1] Emilia L W, Yue X F, Cheng J, Li H and Zhang Y Q 2010 *Chin. Phys. B* **19** 043401
[2] Zhou X, Zhang X, Liu A F and Zeng X H 2010 *Acta Phys. Sin.* **59** 5128 (in Chinese)
[3] Yu Y J, Xu Q and Xu X W 2011 *Chin. Phys. B* **20** 123402
[4] Liu Y F, Liu Y L and Liang B 2012 *Chin. Phys. B* **21** 098201
[5] Xu Z H and Zong F J 2011 *Chin. Phys. B* **20** 063104
[6] Zhao J, Xu Y and Meng Q T 2010 *Chin. Phys. B* **19** 063403
[7] Morley C 1981 *Proceedings of the* 18*th Symposium on Combustion,* August 17–22, 1981, Pittsburgh, USA, p. 23
[8] Baulch D L, Cobos C J, Cox R A, Esser C, Frank P, Just T, Kerr J A, Pilling M J, Troe J, Walker R W and Warnatz J 1992 *J. Phys. Chem. Ref. Data* **21** 411
[9] Koshi M, Yoshimura M, Fukuda K, Matsui H, Saito K, Watanabe M, Imamura A and Chen C 1990 *J. Chem. Phys.* **93** 8703
[10] Davidson D F and Hanson R K 1990 *Int. J. Chem. Kin.* **22** 843
[11] Adam L, Hack W, Zhu H, Qu Z W and Schinke R 2005 *J. Chem. Phys.* **122** 114301
[12] Xu Z F, Fang D C and Fu X Y 1997 *J. Phys. Chem. A* **101** 4432
[13] Zhang S and Truong T N 2000 *J. Chem. Phys.* **113** 6149
[14] Pascual R Z, Schatz G C, Lendvay G and Troya D 2002 *J. Phys. Chem. A* **106** 4125
[15] Poveda L A and Varandas A J C 2005 *Phys. Chem. Chem. Phys.* **7** 2867
[16] Zhai H S and Han K L 2011 *J. Chem. Phys.* **135** 104314
[17] Jordan M J T, Thompson K C and Collins M A 1995 *J. Chem. Phys.* **102** 5647
[18] Thompson K C and Collins M A 1997 *J. Chem. Soc. Faraday Trans.* **93** 871
[19] Thompson K C, Jordan M J T and Collins M A 1998 *J. Chem. Phys.* **108** 8302
[20] Bettens R P A and Collins M A 1999 *J. Chem. Phys.* **111** 816
[21] Knowles P J and Werner H J 1985 *Chem. Phys. Lett.* **115** 259
[22] Werner H J and Knowles P J 1985 *J. Chem. Phys.* **82** 5053
[23] Werner H J and Knowles P J 1988 *J. Chem. Phys.* **89** 5803
[24] Knowles P J and Werner H J 1988 *Chem. Phys. Lett.* **145** 514
[25] Knowles P J and Werner H J 1992 *Theor. Chim. Acta* **84** 95
[26] Han B R, Yang H, Zheng Y J and Varandas A J C 2010 *Chem. Phys. Lett.* **493** 225
[27] Rabitz H and Alis O F 1999 *J. Math. Chem.* **25** 197
[28] Han K L, He G Z and Lou N Q 1996 *J. Chem. Phys.* **105** 8699
[29] Li R J, Han K L, Li F E, Lu R C, He G Z and Lou N Q 1994 *Chem. Phys. Lett.* **220** 281
[30] Aoiz F J, Brouard M and Enriquez P A 1996 *J. Chem. Phys.* **105** 4964
[31] Shafer-Ray N E, Orr-Ewing A J and Zare R N 1995 *J. Phys. Chem. A* **99** 7591
[32] Varandas A J C 1993 *J. Chem. Phys.* **99** 1076
[33] Sayós R, Hernando J, Puyuelo M P, Enríquez P A and González M 2001 *Chem. Phys. Lett.* **341** 608